Simulation of field-emitted electron trajectories and transport from carbon nanotubes

D. G. Walker[a)]
Department of Mechanical Engineering, Vanderbilt University, Nashville, Tennessee 37235-1592

W. Zhang and T. S. Fisher[b)]
School of Mechanical Engineering, and Birck Nanotechnology Center, Purdue University, West Lafayette, Indiana 47907-1288

(Received 7 November 2003; accepted 5 April 2004; published 17 May 2004)

Carbon nanotubes exhibit excellent field-emission behavior characterized by low turn-on fields and large current densities. The present work investigates the transport of electrons by field emission and the resulting spatial distribution at the anode surface through simulation of the tunneling process and the trajectory of electrons across the vacuum gap. Beam spreading is characterized by a multidimensional potential, Coulomb interaction, and randomized energy distributions for closed and open single-walled nanotubes. Electron trajectories are determined by Monte Carlo simulation. Results indicate that the electron beam spreads primarily due to local field curvature near the emission site and that, for some nanotubes, a ring pattern at the anode is created. The ring diameter at the anode spreads by 1.2 μm per 10 μm of vacuum gap for the low currents (<100 μA) considered in this work. These results are consistent with experimental observations. © *2004 American Vacuum Society.* [DOI: 10.1116/1.1755214]

I. INTRODUCTION

Recent advances in patterned arrays of field emission microtips have spurred interest in devices that range from flat-panel displays to efficient power conversion devices.[1,2] The ability to control the size and shape of emitters has allowed researchers to produce highly localized emission because of local field enhancement. Enhancement results in large current densities in cathodes and anodes. Carbon-based materials are particularly advantageous for field emission devices involving high current densities because of their chemical inertness and electrical properties. Polycrystalline diamond emitters exhibit high current density at low applied fields,[3] and monolithic three-terminal devices based on molded diamond nanotip emitters have been shown to produce excellent transistor behavior.[4]

Recent research on carbon nanotubes suggest that they can support local current densities as high as 10^9 A/cm^2,[5,6] and experiments suggest that field emission current densities from emitter arrays could exceed 10^5 A/cm^2.[7] Carbon nanotubes are also very efficient field emitters, with turn-on fields below 5 V/μm.[8] Interestingly, the cross-sectional current from single-walled carbon nanotubes (SWNTs) can exhibit a ring-like current density, indicative of emission from the nanotube edge.[7,9] This behavior produces extremely large local current densities within the ring. The present work simulates transport of emitted electrons across a vacuum gap. The simulation characterizes emission from carbon nanotubes (CNTs) including space-charge effects and enhanced electrical fields to predict ring-like and other structures observed in carbon nanotube emission experiments.

[a)]Author to whom correspondence should be addressed; electronic mail: greg.walker@vanderbilt.edu
[b)]Electronic mail: tsfisher@purdue.edu

Field emission involves quantum tunneling through a potential barrier into vacuum. The probability of electron tunneling is governed by the width of the barrier at a given electron energy. Protrusions from a flat surface provide local field enhancement,[10] which reduces the barrier width and increases the probability of emission. Figure 1 identifies the pertinent parameters of the field emission mechanism important to the present work. Aligned carbon nanotubes naturally provide significant enhancement, which explains, at least in part, their inherent low turn-on voltage and high current density. Emitted electrons are accelerated by an applied field across the vacuum gap and impact the anode. Bombardment of the anode with energetic electrons results in large heating rates in the anode. For devices designed to carry large current densities, anode heating can cause erosion or catastrophic failure of a device.[11] In anode heating studies,[12] the deposition of energetic electrons at the anode is crucial to understanding the thermodynamics of field emitters as well as the potential for damage.

Ring-like emission patterns have been observed in experiments on SWNTs. Zhu *et al.*[7] have suggested that the electron distribution observed from carbon nanotube emission reveals the momentum distribution of electrons leaving the individual emission sites. However, several additional effects are likely responsible for the spreading, including multidimensional potential fields and Coulomb interactions in vacuum. The radial component of the field at the tip of a carbon nanotube can be significant.[13] This accelerating force directs electrons away from the centerline, preserving any ring shape that is created at the emission site.

Additionally, Coulomb interactions among emitted electrons provide a net outwardly radial component to all electrons, further preserving the ring structure. Because the force due to like charges decreases rapidly with distance, electron-

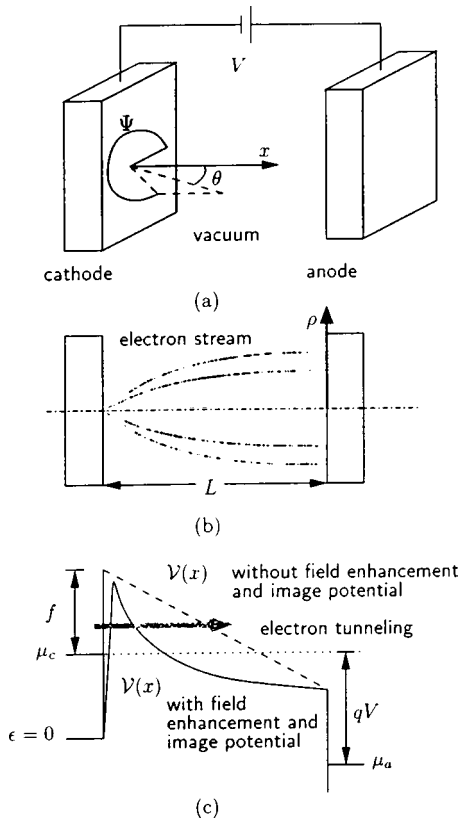

FIG. 1. Schematic representation of field emission between a cathode and anode separated by vacuum. (a) Sketch of planar cathode and anode showing spherical-polar coordinate system at the cathode surface. (b) Side-view schematic of the electron stream and radial coordinate at the anode surface. (c) Electron potential energy distribution from cathode to anode.

induced fields are too small to approach space-charge-limited field-emission conditions.[14] Nevertheless, the initial proximity of the electrons upon emission may be close enough to establish a significant radial velocity component. Recent simulations by Mayer *et al.*[15–17] employ an atomistic transfer matrix method to simulate emission from several types of carbon nanotubes. These simulations, however, assume a uniform electric field in the vicinity of the tip and therefore exclude the spreading effects considered herein.

Through Monte Carlo simulation, the present work seeks to isolate the mechanism that is primarily responsible for beam spreading and preservation of the observed ring-like pattern from CNTs. The mechanisms examined include Coulomb interactions among electrons, nonaxial field at the CNT tip, and random nonaxial momentum components of the electrons at emission. Both emission and acceleration of the electrons depend intimately on the potential in the vacuum gap. Therefore, the potential field for a floating sphere between two parallel plates is presented and used to model a close-ended nanotube, and a different analytic mapping of the floating sphere model is presented to obtain the potential at the open nanotube end (rod). The energy distribution at the anode is studied for further anode heating studies.

II. THEORY

Field emission from flat metallic surfaces was first characterized by Fowler and Nordheim.[18] Good and Müller[19] provided a comprehensive review of the theory from first principles. Even though the Fowler–Nordheim expression is strictly valid for flat emitters only, the extension to geometrically enhanced cathodes has been made by introducing a field enhancement factor. This factor represents the effective slope of the enhanced potential at the cathode surface compared to the potential of a flat surface with the same applied voltage and gap width. Note that this approximation does not satisfy the anode boundary condition; it is simply a linearization of the field at the cathode. Because the present work focuses on the acceleration of the electrons across the entire gap, a more accurate representation of the field in the vacuum gap is required.

The current density J of field-emitted electrons can be calculated from the following general integral:

$$J = q\int_{-W_a}^{\infty} D(W)N(W)dW, \tag{1}$$

where q is the magnitude of the electron charge, $-W_a$ represents the bottom of the emitter's conduction band, W is the component of electron energy flux in the emission direction, $N(W)dW$ is the electron supply function, and $D(W)$ is the quantum tunneling transmission coefficient.

The transmission coefficient $D(W)$ represents the probability that an electron will tunnel from the solid into vacuum. The transmission coefficient depends strongly on the width of the potential barrier encountered by the electron. In the present work, we employ the Wentzel–Kramers–Brillouin approximation for the transmission coefficient[19]

$$D(W) = \exp\left[-\int_{x_1}^{x_2}\sqrt{\frac{8m}{\hbar^2}|\mathcal{V}(x)-W|}\,dx\right], \tag{2}$$

where x_1 and x_2 are the zeroes of $\mathcal{V}(x)-W$ such that $x_2 - x_1$ represents the local width of the barrier.

For tunneling and electron trajectory calculations, the potential profile $\mathcal{V}$ is a critical parameter. Traditional Fowler–Nordheim theory employs a one-dimensional potential field. Here we employ a three-dimensional field with radial symmetry. Prior studies[20–22] have shown that a floating sphere model can approximate, to a reasonable accuracy, the local electric field near the surface of a field emitter with a sharp tip. The resulting potential profile follows:

$$\mathcal{V}(r,\theta) = -qF_0 r\left(1-\frac{a^3}{r^3}\right)\cos\theta + qF_0 h\left(\frac{a}{r}-1\right) - \frac{q^2 a}{8\pi\epsilon_0(r^2-a^2)}\,\frac{K-1}{K+1}, \tag{3}$$

where r is the radial coordinate measured from the sphere's center, θ is the polar angle, F_0 is the uniform electric field far from the sphere, and a is the sphere radius. The last term in Eq. (3) represents image potential, where K is the dielectric constant, q is the electron charge, and ϵ_0 is the permittivity

of free space. For the one-dimensional tunneling calculation of Eq. (2), the local potential along the surface normal is used. The three-dimensional potential is employed for electron dynamics calculations, as discussed later.

To improve the approximate potential near an open-ended carbon nanotube, a conformal map is used to transform the potential from the floating sphere model to the flat surface of the end of a rod, or whisker. In this transformation, the spherical coordinates of the floating sphere are converted to radial coordinates such that $\zeta = r\sin\theta$ and $z = r\cos\theta$. Because of the azimuthal symmetry, the two radial coordinates create a complex plane, $w = \zeta + iz$, where the mapping

$$w \mapsto \frac{w + \sqrt{w^2 - a^2}}{2} \tag{4}$$

takes the open-ended CNT coordinates to the floating sphere coordinates. The conformal map can be found in most complex variable analysis texts such as [Ref. 23, p. 371, (ix)]. The transformation is strictly valid for $z > 0$. The potential for the open-ended nanotube is given as

$$\begin{aligned}\mathcal{V}(\zeta,z) &= F_0\left[\frac{8a^3}{|\zeta+iz+\sqrt{(\zeta+iz)^2-a^2}|^3}-1\right] \\ &\quad + F_0 h\left[\frac{2a}{|\zeta+iz+\sqrt{(\zeta+iz)^2-a^2}|}-1\right] \\ &\quad \times\left[\frac{z}{2}+\frac{1}{2}\,\mathrm{Im}\left(\sqrt{(\zeta+iz)^2-a^2}\right)\right] \\ &\quad - \frac{q^2}{8\pi\epsilon_0}\frac{K-1}{K+1}\left[\frac{|\zeta+iz+\sqrt{(\zeta+iz)^2-a^2}|}{2a^2-\frac{1}{2}|\zeta+iz+\sqrt{(\zeta+iz)^2-a^2}|^2}\right],\end{aligned} \tag{5}$$

where $\mathrm{Im}(w)$ is the imaginary component of the complex number w, and $|w|$ is its magnitude. Note that the radius, a, in Eqs. (4) and (5) should be one-half of the physical tip radius used in Eq. (3), due to the transformation.

Immediately upon emerging from the tunneling barrier, an electron's initial axial location is determined from the known potential energy and potential profile. In the present work, we consider two possible scenarios: (1) emission from the hemispherical cap of a closed SWNT tip and (2) emission from an open SWNT. In the former case, emission sites are chosen based on the calculated current density from the one-dimensional emission model. In the latter case, emission occurs uniformly over the CNT end. Further, for both cases, the effect of the tangential component of kinetic energy is studied by randomly choosing non-normal energies with a maximum magnitude of $k_B T$, where $T = 300\,\mathrm{K}$. In both cases, the direction and energy are randomized.

Electron transport from cathode to anode is treated classically. Trajectories are predicted using a Monte Carlo simulation,[24] which includes the Coulomb interaction of electrons in vacuum and the acceleration due to potential field $\mathcal{V}(r,\theta)$. Predicting the trajectories of electrons using Monte Carlo involves summation of forces on particles to calculate accelerations. The forces include electric field components from the applied voltage and space charge. The simulation involves discrete time stepping such that higher-order terms in the Taylor series expansion of the location and velocity at $t+\Delta t$ are omitted. The size of the time step required is inversely proportional to the order of terms used in the calculations. However, higher-order terms increase the computational requirements of the simulation. Because the applied field is assumed to be constant, an exact solution can be obtained with a second-order expansion for location and a first-order expansion for velocity in the absence of other forces.

Given an ensemble of particles with known location ($\mathbf{r}_i$) and velocity vectors ($\mathbf{v}_i$) at time t, new positions and velocities at time $t+\Delta t$ can be found from the expansions

$$\begin{aligned}\mathbf{r}_i(t+\Delta t) &= \mathbf{r}_i(t) + \mathbf{v}_i(t)\Delta t + \tfrac{1}{2}\mathbf{v}_i'(t)\Delta t^2 + \tfrac{1}{6}\mathbf{v}_i''(t)\Delta t^3 \\ &\quad + \mathcal{O}(\Delta t^4),\end{aligned} \tag{6}$$

$$\mathbf{v}_i(t+\Delta t) = \mathbf{v}_i(t) + \mathbf{v}_i'(t)\Delta t + \tfrac{1}{2}\mathbf{v}_i''(t)\Delta t^2 + \mathcal{O}(\Delta t^3). \tag{7}$$

The first time derivative of velocity (i.e., acceleration) is found from summation of forces on each particle

$$\mathbf{v}_i'(t) = \frac{qE}{m} + \frac{C_0}{m}\sum_{j\neq i}^{N_{e^-}}\frac{\mathbf{r}_{ij}}{|\mathbf{r}_{ij}|^3}. \tag{8}$$

Here, the first term is the force on the particle by the applied field, the second term is the space charge between each particle and all its neighbors such that $q = 1.6\times10^{-19}\,\mathrm{C}$ is the charge of an electron, $\epsilon_0 = 8.85\times10^{-12}\,\mathrm{F/m}$ is the permittivity of free space, $m = 9.1\times10^{-31}\,\mathrm{kg}$ is the mass of an electron, and $C_0 = q^2/4\pi\epsilon_0$. Because the applied field is assumed constant, time derivatives of qE are zero and the second order time derivative of velocity is given as

$$\mathbf{v}_i''(t) = \frac{C_0}{m}\sum_{j\neq i}^{N_{e^-}}\left[\frac{\mathbf{v}_{ij}}{|\mathbf{r}_{ij}|^3} - \frac{3(\mathbf{r}_{ij}\cdot\mathbf{v}_{ij})\mathbf{r}_{ij}}{|\mathbf{r}_{ij}|^5}\right]. \tag{9}$$

The rate of emission of electrons is governed by the one-dimensional field emission model integrated over the emitter surface. For a given total current, the average number of electrons in vacuum can be approximated by

$$\langle N\rangle = \frac{\Delta t_{\mathrm{vac}} I}{q}. \tag{10}$$

The time required for a single electron to cross the gap depends on the acceleration produced by the applied voltage

$$\Delta t_{\mathrm{vac}} = \sqrt{\frac{2(L-h)^2 m_e}{qV_0}}, \tag{11}$$

where V_0 is the applied voltage, L is the cathode anode distance, h is the tube height, m_e is the mass of an electron, and q is the charge of an electron. The actual acceleration near the tip will be slightly larger due to space-charge effects and field enhancement. Therefore, the linear-field approximation

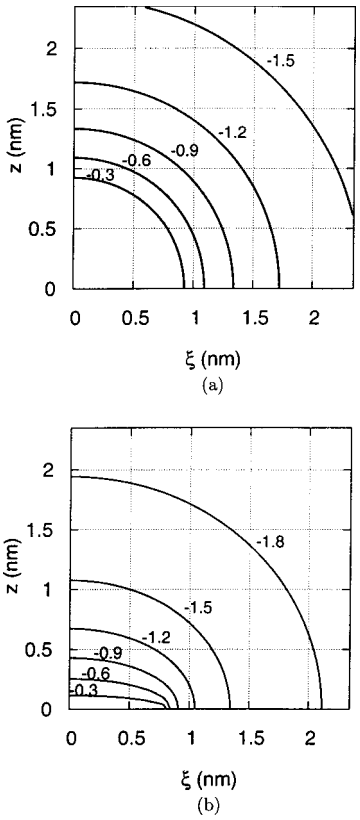

FIG. 2. Potential contours immediately above a nanotube for both the floating sphere model (a) and the rod model (b) near the tube end for tube diameter of 1.6 nm. In both cases, the applied field is 1.4 V/μm, and the current is 40 nA. The tube centerline corresponds with the z axis and the contours are labeled in volts.

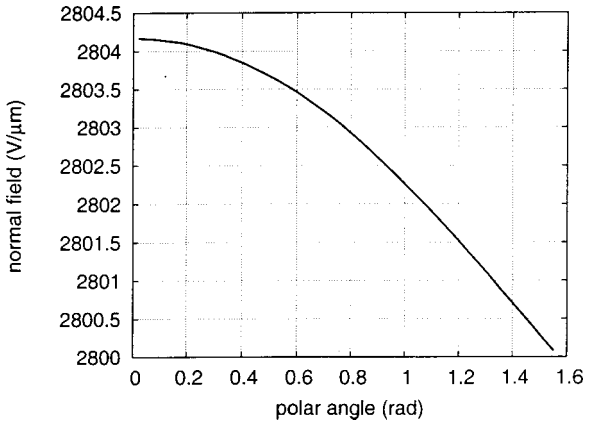

FIG. 3. Local field normal to capped surface at end of carbon nanotube as a function of polar angle measured from the tube axis.

will overestimate the number of electrons in the gap. Nevertheless, the time in Eq. (11) provides an upper bound on the simulation time step.

The free-flight of each electron in the gap is predicted including Coulomb interactions with all other electrons. As the electrons pass the anode boundary, they are removed from the simulation. The anode was spatially discretized so that electron energy and location could be recorded. The current density is obtained for each bin by counting the number of electrons (n) in these bins

$$J_{\text{bin}}=\frac{qn}{t_{\text{sim}}A_{\text{bin}}}, \tag{12}$$

where A_{bin} is the area of the bin and t_{sim} is the total simulation time.

III. RESULTS

We first consider a capped nanotube where the end is modeled as a hemisphere. The potential is given by Eq. (3) and shown in Fig. 2 for an applied field of 1.4 V/μm and work function of 4.5 eV. The height of the tube is $h=1.6\,\mu$m and the diameter is $2a=1.6$ nm. The field normal to the surface of the hemispherical cap, shown in Fig. 3, varies with the polar angle by less than a percent. Therefore, for the present analysis, the transmission is assumed to be constant at all points on the surface of the capped end. The magnitude of the local normal field $F\approx 2800$ V/μm suggests that an appropriate unitless form of the Fowler–Nordheim geometric field enhancement would be $\beta\approx 2000$. This value is consistent with experimental findings.[25] Further, from *ab initio* studies, Han and Ihm[26] predicted a field enhancement of $\beta\sim 1000$ for a 1.4 nm diameter carbon nanotube with a similar applied field. The apparent discrepancy is likely due to the self-consistent calculation of the external field in the *ab initio* calculation. The *ab initio* formulation does not account rigorously for cathode or anode boundary conditions and actual tube length. Nevertheless, local fields are of the order of *ab initio* studies.[27]

Based on the local normal field on the cap surface (from Fig. 3), Fowler–Nordheim emission predicts a current density of $j=10$ A/cm^2 at the centerline that decreases by 2% at the cap edge (polar angle of $\pi/2$). If we assume that emission occurs uniformly across the surface of the cap, the total current from a single nanotube is approximately 4.2×10^{-4} nA. If the field is increased to 2.3 V/μm (almost doubled), the current becomes 7.6 nA, which is consistent with measured values.[7]

Upon emission, we can determine where the electrons will impact the anode based on the field between the nanotube and the anode. For special cases, an analytic transformation can be obtained to predict the spatial distribution of current at the anode.[28] However, for the present case, the electron trajectories and distribution at the anode is solved numerically. In the absence of initial energy and Coulomb interactions, electrons are traced from the cap to the anode. Figure 4 shows the radial location of electrons impacting the anode as a function of emitted polar angle for a vacuum gap of 500 μm. This plot suggests that the electrons emitted from the edges of the cap (large polar angle) will deposit at similar radial locations at the anode. Therefore, if emission were uniform on the hemisphere, we might expect a ring of large current density at 55 μm. However, the actual current density is a function of the area as well. Using Fig. 4, we can calculate a ratio of hemispherical area to anode area for points at different polar angles on the capped end. Current densities at

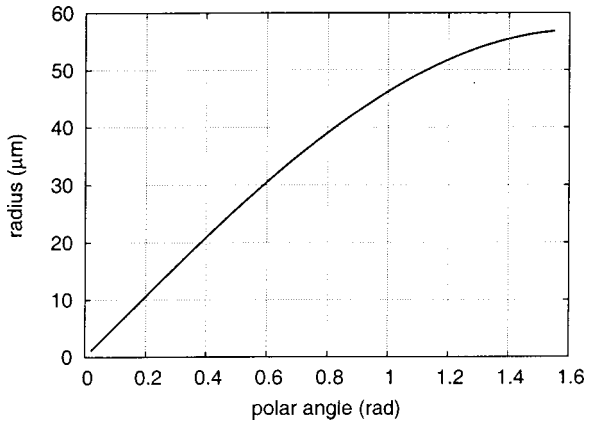

FIG. 4. Radial location on the anode of an electron impact given emission from a particular polar angle.

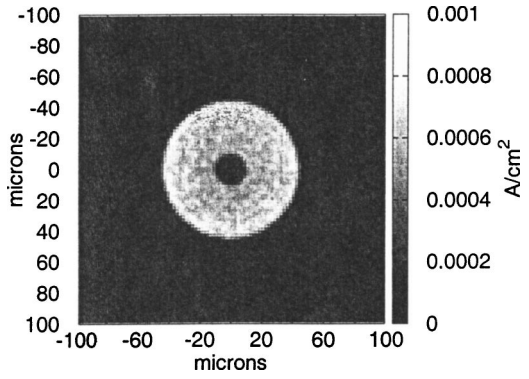

FIG. 6. Current density at the anode for emission from a hemispherical tip emitting between polar angles of 10° to 50°. The applied field is 1.4 V/μm and the zero datum point is the beam centerline.

the anode are simply the nominal Fowler-Nordheim current density times the area ratio. Figure 5 shows the expected current density at the anode given no initial energy and no Coulomb interaction (ideal). Based on these data, we see a strong ring appearing at the anode 55 μm from the centerline of the nanotube as expected.

The foregoing analysis does not include the fact that electrons may emit with momentum components that are perpendicular to the surface normal. Results from *ab initio* studies[27] indicate that the emitted electron can have velocity components that are not parallel to the potential streamlines (surface normal at the tip). To introduce this feature into the foregoing simulation, an initial velocity was randomly chosen with an outwardly normal component. The magnitude is also randomly chosen and is based on the kinetic equation and the thermal energy

$$k_B T = \tfrac{1}{2} m v_i^2, \tag{13}$$

where k_B is the Boltzmann constant, m is the rest mass of an electron, v_i is the initial velocity, and T is the nanotube temperature.

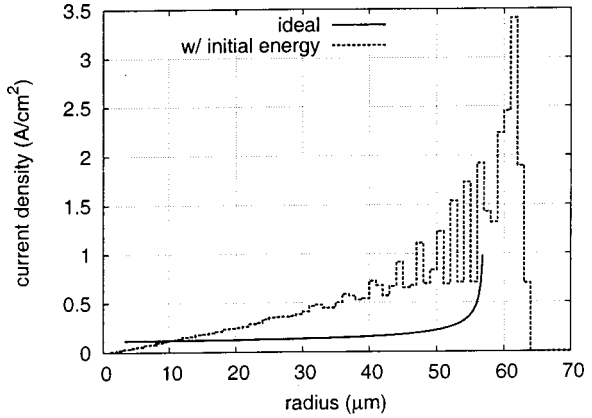

FIG. 5. Current density as a function of radius at the anode for emission from a closed nanotube with uniform emission over the hemispherical tip. The applied field is 1.4 V/μm.

To obtain current densities at the anode with an initial velocity, the location of emission was chosen randomly on the surface of the hemisphere. Figure 5 shows the intensity (current density) of electrons at the anode with some initial kinetic energy compared to the ideal case described earlier. Once this ''thermal noise'' is introduced into the simulation, the ring radius increases to 62 μm. Further, the intensity near the centerline decreases because any initial velocity of electrons near the centerline will be oriented away from the centerline. It should be noted that the integral of both plots is the same (4.2×10^{-4} nA) even though the area under the curves do not look equivalent. Once the current density is scaled by the area, which gives current, both curves result in the same current.

An additional image was generated from the data so that a visual comparison to phosphor data could be made (Fig. 6). These results assume uniformly distributed emission over the hemispherical area of the cap. *Ab initio* studies of carbon nanotubes show that emission occurs in a distinct ring for a capped tube.[27] Because the transmission is approximately uniform, the ring loosely represents the density of electrons available for emission. Based on density images from Ref. 27, emission was restricted to polar angles between 10° and 50°. The ''flower petals'' occasionally seen on phosphor screens were ignored because the intensity in these regions was low and the inclusion of these regions will not significantly affect the ring size. The ratio of inner radius to outer radius (24%) compares well to that of Han and Ihm.[27] The ring diameter of 90 μm is within a few percent of data from Zhu *et al.*[9] for similar voltages and vacuum gap. It should be noted that the tubes in Zhu's data contain a mix of capped and open nanotubes of varying diameters and lengths. Therefore, the agreement is perhaps fortuitous. The fact that rings observed by Zhu have larger inner to outer diameter ratios might be a result of the turn-on threshold of the phosphor.

The analysis of the open-ended nanotube proceeds by assuming that the electrons available for emission are distributed uniformly across the end of the tube. Effective screening of the field inside the tube from first-principles and comparisons of total and local density of states[26] suggest that this assumption is reasonable. Unlike the capped nanotube,

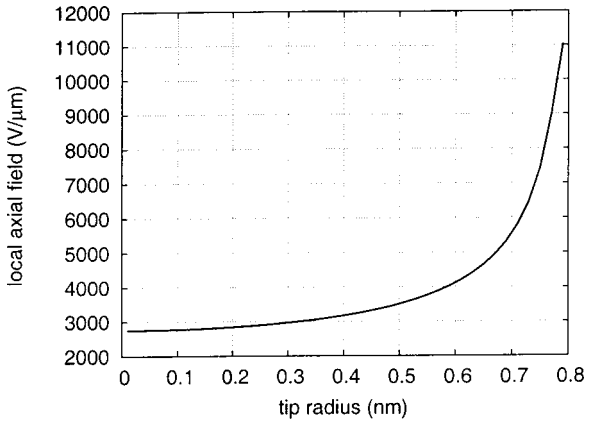

FIG. 7. Electric field based on potential from Fig. 2(b) as a function of radial location on the tip. The applied field is 1.4 V/μm.

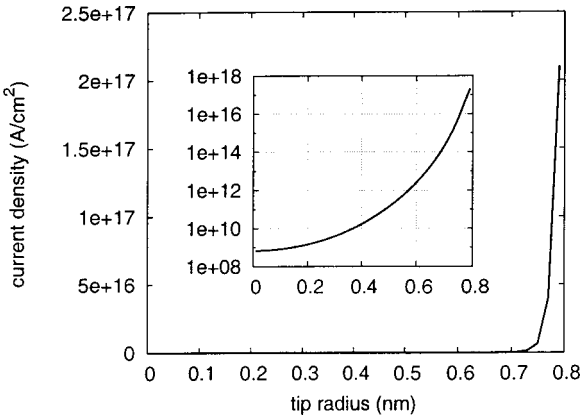

FIG. 9. Emission from the nanotube end along the radius of the tip. The applied field is 1.4 V/μm. The inset contains the same data on a log scale, and the units for both views are the same.

the field varies greatly across the radius of open-ended tube. Figure 7 shows a fourfold increase in the field at the edge compared to the centerline. The nanotube edge causes the enhancement to be magnified as seen in Fig. 2(b). Also, the radial component of the field is relatively small near the centerline compared to the edge. Consequently, electrons originating from the interior of the tube will spread relatively little compared to those that originate near the edge. In fact, Fig. 8 shows the opposite trend from the capped tube (compare to Fig. 4).

Because the field varies significantly across the tip radius, the emission will also vary significantly. Fowler–Nordheim emission based on the local field results in several orders of magnitude variation in the emission, which is greatest at the tube edge. In fact, the dependence on radial location is stronger than an exponential relationship (see inset of Fig. 9 for nonlinear behavior on a log scale). Therefore, it is reasonable to assume that electrons are emitted at the tube edge only. Since the field has a radially outward component, the ring should be preserved as the electrons accelerate in vacuum toward the anode. Also notice that the current density is much greater than the capped nanotube, but the total current could be nearly equal because the area for emission on the open ended tube is presumably much smaller.

Figure 10 shows the simulated phosphor image generated by emission from an open-ended nanotube with initial kinetic energy. The energy was assumed to be at the maximum thermal energy (0.0259 eV) with random initial direction, as in the capped tube case. The difference in the inner (75 μm) and outer diameters (110 μm) of the ring is a result of the random initial energy only. Also note that the current density is relatively uniform across the ring. This pattern agrees well with Zhu's measurements,[7] including the ring size.

IV. CONCLUSIONS

Observed anode ring patterns that represent current density of electrons emitted from carbon nanotubes have been simulated using a Monte Carlo approach. Two tube configurations were considered (open-ended and capped tubes), and the emission at the tube ends was approximated using standard one-dimensional emission models. Simulated results indicate that both configurations will likely produce ring patterns at an anode. However, the mechanism for ring production is entirely different. In the case of the closed tube, the density of electrons available for emission affects the

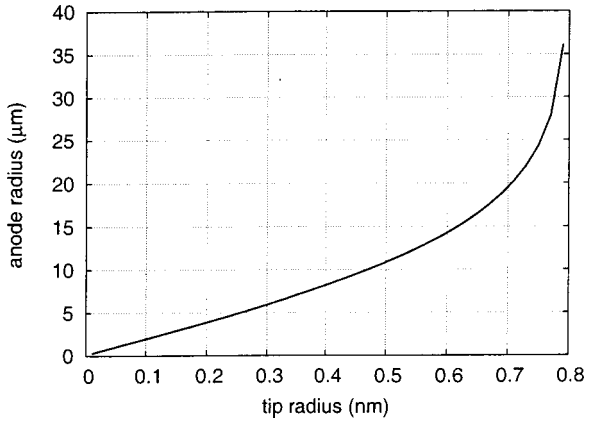

FIG. 8. Electrons that are emitted from a radial location on the tip (abscissa) impact at a radial location on the anode (ordinate).

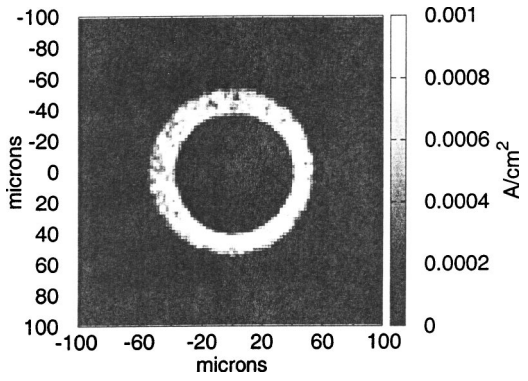

FIG. 10. Current density at the anode for emission from a open-ended nanotube emitting at the tip edge only. The applied field is 1.4 V/μm and the zero datum point is the beam centerline.

location of emission. For the open tube, emission is possible only where the field is large enough to produce enhancement, which occurs near the tube edges. In both cases, the ring that is created upon emission is preserved as the electrons travel in vacuum and impact the anode.

The features that affect the ring size, location and intensity at the anode are initial kinetic energy of the emitted electron and the multidimensional field. In the case of the open tube, the field calculation very near the tube edge is somewhat dubious because of the mathematical singularity. Detailed self-consistent calculations should be performed to evaluate the density and the local field at the open tube end. Nevertheless, both configurations match remarkably well with observed and measured data published elsewhere.

ACKNOWLEDGMENTS

This work was supported in part by an NSF Career Award No. (CTS-9983961), a Vanderbilt University Discovery Grant, a NSF NIRT grant, and DARPA/ARO's Palm Power program.

[1]I. Brodie and P. R. Schwoebel, Proc. IEEE **82**, 1006 (1994).
[2]J. A. Nation, L. Schachter, F. M. Mako, L. K. Len, W. Peter, C.-M. Tang, and T. Srinivasan-Rao, Proc. IEEE **87**, 865 (1999).
[3]W. P. Kang, T. S. Fisher, and J. L. Davidson, New Diamond Front. Carbon Technol. **11**, 129 (2001).
[4]A. Wisitsora-at, W. P. Kang, J. L. Davidson, D. V. Kerns, and T. S. Fisher, J. Vac. Sci. Technol. B **21**, 614 (2003).
[5]S. B. Sinnott and R. Andrews, Crit. Rev. Solid State Mater. Sci. **26**, 145 (2001).
[6]M. S. Dresselhaus, Science **292**, 650 (2001).
[7]W. Zhu, C. Bower, O. Zhou, G. P. Kochanski, and S. Jin, Appl. Phys. Lett. **75**, 873 (1999).
[8]J.-M. Bonard, H. Kind, T. Stockli, and L. A. Nilsson, Solid-State Electron. **45**, 893 (2001).
[9]W. Zhu, C. Bower, G. P. Kochanski, and S. Jin, Diamond Relat. Mater. **10**, 1709 (2001).
[10]C. A. Spindt, J. Appl. Phys. **39**, 3504 (1968).
[11]P. Grant, C. Py, C. Mössner, A. Blias, H. Tran, and M. Gao, J. Appl. Phys. **87**, 1356 (2000).
[12]D. G. Walker and T. S. Fisher, Proceedings of the International Mechanical Engineering Congress and Exposition, number 32126, November 2002.
[13]J. D. Zuber, J. Appl. Phys. **91**, 9379 (2002).
[14]A. E. Bell and L. W. Swanson, Phys. Rev. B **19**, 3353 (1979).
[15]A. Mayer, N. M. Miskovsky, and P. H. Cutler, J. Vac. Sci. Technol. B **20**, 100 (2002).
[16]A. Mayer, N. M. Miskovsky, and P. H. Cutler, Phys. Rev. B **65**, 195416 (2002).
[17]A. Mayer, N. M. Miskovsky, and P. H. Cutler, Ultramicroscopy **92**, 215 (2002).
[18]R. H. Fowler and L. W. Nordheim, Proc. R. Soc. London, Ser. A **119**, 173 (1928).
[19]R. H. Good and E. W. Müller, in *Encyclopedia of Physics*, edited by S. Flugge (Springer, Berlin, 1956), Vol. 21, pp. 176–231.
[20]T. Utsumi, IEEE Trans. Electron Devices **38**, 2276 (1991).
[21]K. L. Jensen, E. G. Zaidman, M. A. Kodis, B. Goplen, and D. N. Smithe, J. Vac. Sci. Technol. B **14**, 1942 (1996).
[22]J.-M. Bonard, K. A. Dean, B. F. Coll, and C. Klinke, Phys. Rev. Lett. **89**, 197602 (2002).
[23]J. E. Marsden and M. J. Hoffman, *Basic Complex Analysis*, 2nd ed. (Freeman, New York, 1987).
[24]G. H. Jansen, Nucl. Instrum. Methods Phys. Res. A **298**, 496 (1990).
[25]J.-M. Bonard, J.-P. Salvetat, T. Stöcklii, W. A. de Heer, L. Forró, and A. Châtelain, Appl. Phys. Lett. **73**, 918 (1998).
[26]S. Han and J. Ihm, Phys. Rev. B **61**, 9986 (2000).
[27]S. Han and J. Ihm, Phys. Rev. B **66**, 241402 (2002).
[28]T. S. Fisher, D. G. Walker, and R. A. Weller, IEEE Trans. Compon. Packag. Manuf. Technol. **26**, 317 (2003).